Journal of Porphyrins and Phthalocyanines
J. Porphyrins Phthalocyanines 2011; **15**: 277–292
DOI: 10.1142/S1088424611003264

Published at http://www.worldscinet.com/jpp/

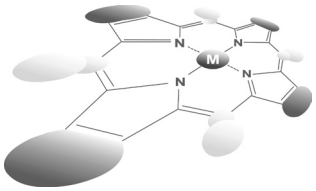

The synthesis and characterization of a side-by-side iron phthalocyanine dimer

Wei He and Marya Lieberman*◊

Department of Chemistry and Biochemistry, University of Notre Dame, Notre Dame, IN 46556, USA

Received 30 March 2011
Accepted 1 May 2011

ABSTRACT: The QCA paradigm is one of the approaches to decrease the size scale of computing devices. When molecules are used as QCA cells, they may be able to perform computing at room temperature. This paper describes a novel molecular QCA cell candidate which is a side-by-side iron phthalocyanine dimer, and an investigation of its optical and redox properties. The new dodeca(pentyloxy) substituted side-by-side iron phthalocyanine dimer, along with the octa(pentyloxy) iron phthalocyanine monomer, are soluble in non-polar organic solvents. These compounds were isolated by gel permeation chromatography (GPC) and high-performance liquid chromatography (HPLC) to final purities of 98% and 99%, respectively. The NMR spectra of both compounds in $CDCl_3$ are broad due to aggregation, but become well resolved after the addition of the coordinating solvent pyridine-d_5. Addition of pyridine also gives changes in the UV-vis spectra and electrochemical peaks of both monomer and dimer in dichloromethane indicative of axial iron coordination. The electrochemical data indicates the loss of pyridine ligands from the oxidized products of both monomer and dimer. The comproportionation constant of side-by-side phthalocyanine dimer shows that its oxidized and reduced mixed-valence complexes are fairly stable. The dimer is thus a candidate for molecular QCA systems.

KEYWORDS: iron phthalocyanine, Fe phthalocyanine, pc, dimer, aggregation, HPLC, electrochemistry, UV-vis, NMR, mass spectrometry, pyridine.

INTRODUCTION

The quantum-dot cellular automata (QCA) concept is a paradigm for transmitting and processing information in arrays of quantum dots. The positions of charges in the quantum dot array are used to perform logical computations. According to the QCA theory [1, 2], the smaller the quantum dots are, the better they can work as charge containers; when the cell dimensions approach molecular sizes, it is predicted that room temperature operation, very high speed, and low energy consumption can all be achieved [3]. In the QCA paradigm, each cell is field-coupled to its neighbors so that individual contacts to the cells are not necessary, which is particularly attractive for molecular electronics.

In chemical terms, the smallest possible quantum dot can be thought of as a redox center in a suitable molecule. There are many examples of molecules that contain arrays of redox centers in precise locations, and calculations have shown that a dimeric mixed-valence compound (containing two redox centers connected by a bridging moiety to mediate electron transfer) could be used as an individual QCA cell [1]. Our ultimate goal is to self-assemble molecular QCA cells onto substrates to perform computing. Since self-assembly methods have shown the capability for patterning nanostructures [4–7], and electron beam lithography is capable of making sub-10 nm size structures [8], it may be possible to employ lithography and self-assembly methods to help pattern QCA molecules on the substrates. This paper describes the synthesis and characterization of a pc dimer which is well suited to both QCA function and surface assembly.

Phthalocyanine compounds have, since their first discovery in 1907 and the elucidation of their structure in

◊SPP full member in good standing

*Correspondence to: Marya Lieberman, email: mlieberm@nd.edu, tel: +1 574-631-4665, fax: +1 574-631-6652

1934, achieved a notable success as a model structure for experimental organic, theoretical, and physical chemical study. For many years the insolubility of unsubstituted phthalocyanines hindered studies on their reactivity and properties. The poor solubility results from strong π-stacking interactions between the phthalocyanine rings and weak solvent-phthalocyanine interactions. Kenney's group found that the axial Si-OH bonds in $(OH)_2SiPc$ could react with trialkylchlorosilanes to form bis-siloxy-SiPcs with good solubility in organic solvents [9]. An alternative way to enhance the solubility of pcs in organic solvents was developed by Hanack, who introduced peripheral substitutents into the macrocycle [10]. This provides a convenient way to increase the solubility of the compounds while freeing up the axial positions for other roles.

In order to make phthalocyanine dimers, one can either stack the phthalocyanines one atop the other [11–13], or construct two phthalocyanine rings side-by-side [14–16]. Previous work in our group has explored the stacked dimer geometry [17, 18], but subsequent calculations [19] suggested that a side-by-side dimer would be more suitable for our purposes in fabrication of molecular electronic devices. In particular, the side-by-side dimer would be more accessible for Ultra High Vacuum Scanning Tunneling Microscope (UHV-STM) studies, since both sides of the molecule would be equally exposed atop a solid surface. An iron phthalocyanine was chosen in part because of the rich axial chemistry of the iron [20–22], which could facilitate surface attachment on self-assembled monolayers. A tetra-nitrilo benzene was chosen to form the linker between the two phthalocyanine rings, because the conjugated system facilitates electron delocalization. As seen in molecule **2** in Fig. 1, the two cojoined phthalocyanine rings are expected to share this benzene ring, with an expected distance of 1.2 nm between the two iron atoms. The phthalocyanine rings were decorated with pentyloxy groups in order to increase their solubilities; this was an important synthetic goal both to facilitate characterization of the products, and because surface attachment requires high purity material.

There are generally two strategies for making unsymmetrical phthalocyanines; the ring expansion method and the statistical method. The ring-expansion method utilizes boron subphthalocyanines (B-SubPcs) reacting with diiminoisoindoline analogues [23, 24]. The final yields of unsymmetrical pcs varied from 8–20%. One of the shortcomings of this method is the thermal instability of B-SubPc [25], and in our hands, ring expansion of B-SubPc was not sucessful for generation of the desired FePc dimers.

The other method to make unsymmetrical phthalocyanines is based on condensation of two different *ortho*-dinitriles, giving statistical mixtures of products which must then be purified [26]. Reaction conditions are similar to standard phthalocyanine syntheses: high reaction temperature (> 150 °C), long heating time (> 24 h), and an inert environment (argon or nitrogen gas). 1-chloronaphthalene or *N*,*N*-dimethylaminoethanol (DMAE) is typically used as the solvent. The reported yields of unsymmetrical pcs vary from 1% (unsymmetrical CoPc) [27] to 10% (unsymmetrical ZnPc) [28] to 19% (unsymmetrical NiPc) [29].

Purification of phthalocyanine products is often difficult, yet purity is critical for molecules that will eventually be used for surface deposition studies. Extensive solvent washing and sublimation are commonly used to remove impurities from the relatively insoluble unsubstituted phthalocyanines [30]. For phthalocyanine derivatives with higher molecular weight, the sublimation method is not applicable because peripheral substitutents of the phthalocyanine often fragment during heating. TLC and chromatography on silica are often used to separate phthalocyanine fractions, but the separation that can be achieved is limited by the relatively low number of theoretical plates. Gel permeation chromatography separates

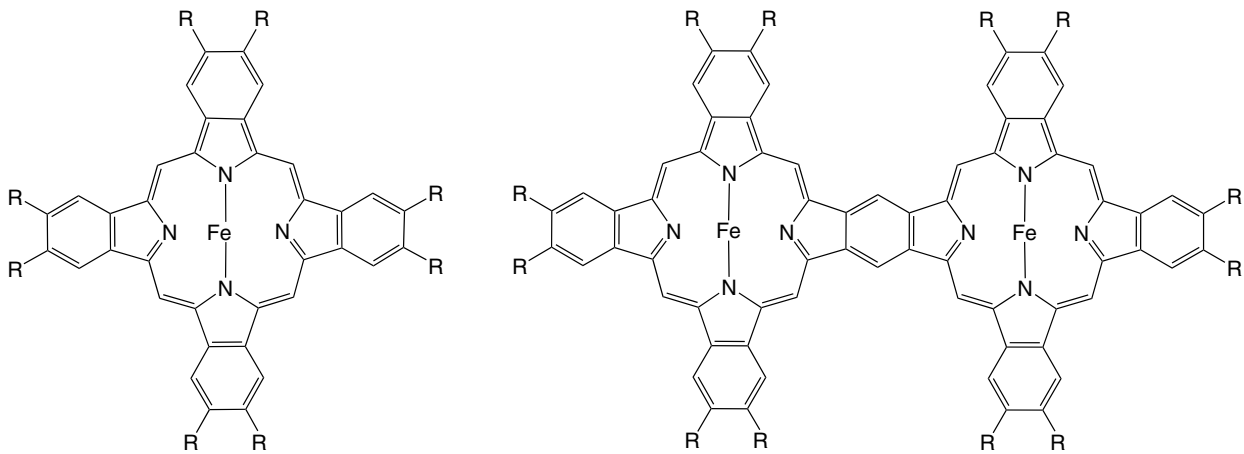

1 **2**

Fig. 1. Molecular structure of iron phthalocyanine monomer **1** and side-by-side iron phthalocyanine dimer **2**

materials on the basis of molecular size, which is useful for removing starting materials from crude pc products and separating products of different molecular weights [31–34]. However, the separation obtained is limited. We turned to high-performance liquid chromatography (HPLC) [35] to achieve better phthalocyanine purity for surface deposition. As a side benefit, the diode-array detector allowed us to identify each fraction as it came out of the stationary phase of the column. **2** was obtained in 12% yield based on 1,2,4,5-tetranitrilobenzene, and analytical HPLC result showed its purity at 98%.

With pure iron octakis(pentyloxy)phthalocyanine monomer (**1**) and side-by-side bis iron dodeca(pentyloxy) phthalocyanine dimer (**2**) (as seen in Fig. 1) in hand, detailed spectroscopic characterization and electrochemical measurements were obtained in organic solvents. We were particularly interested in the effect a strongly coordinating solvent (pyridine) would have on the aggregation state of the phthalocyanines in solution, as we felt that surface deposition would be more likely to yield isolated molecules for STM analysis if the phthalocyanines started out more or less monomeric in solution.

RESULTS AND DISCUSSION

Synthesis

1,2-dicyano-4,5-bis(pentyloxy)benzene (6). The synthesis route for 1,2-dicyano-4,5-bis(pentoxy)benzene is shown in Scheme 1, which is modified from the work done by Hanack [36]. This route starts from the bromination of catechol (**3**) [37]. The yield of the resulting 4,5-dibromocatechol (**4**) is 45%. O-alkylation of **4** with 1-bromopentane in DMF produces dialkyloxy dibromocatechol (**5**, 85%) in good yield in the presence of K_2CO_3 (Hanack used $NaOCH_3$ as the base in this reaction). The aromatic bromide (**5**) was then heated with CuCN in DMF solution, and phthalonitrile (**6**, 59%) was obtained. The overall yield of **6** from catechol was 23%. Copper octa(pentyloxy)phthalocyanine was obtained as a side product in the cyanization reaction.

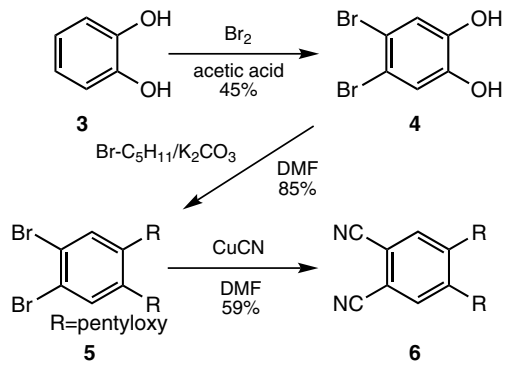

Scheme 1. The synthesis pathway to 1,2-dicyano-4,5-bis(pentyloxy)-benzene (**6**)

Bis-diiminoisoindoline (8). To make the linker for the phthalocyanine dimer, the commercially available 1,2,4,5-tetracyanobenzene (**7**) was bubbled with gaseous ammonia in the presence of sodium methoxide and methanol for 45 min to form bisdiiminoisoindoline (**8**). **8** was insoluble in methanol and precipitated out, giving a yield of 99%. IR was used to confirm the disappearance of the C≡N stretching frequency at 2228 cm^{-1}.

Statistical synthesis of 1 and 2

The ring-expansion [24] of boron sub-phthalocyanine was first attempted to synthesize phthalocyanine dimers, but in our hands it yielded little isolable phthalocyanine product. We believe that the self-condensation of the bisdiiminoisoindoline and degradation of the boron (hexapentyloxy) sub-phthalocyanine at high temperatures hindered the formation of the desired phthalocyanine dimers. The statistical method as shown in Scheme 2 was used to make the pc dimer compound **2** with a yield of 12% based on tetracyananobenzene. One of the major challenges in this approach was to overcome the poor solubility of bisdiiminoisoindoline (**8**). To solve this problem, bisdiiminoisoindoline was first heated in DMAE to boiling point. $FeCl_2 \cdot 4H_2O$ and a DMAE solution of **6** were then added drop-wise from different necks of a 3-neck flask over half an hour. The reaction was done under a blanket of NH_3 gas. This procedure was intended to keep the concentration of **6** low and thus increase the chance for condensation with **8** to form the pc dimer **2**. Still, the pc monomer **1** was the major product and it was hard to separate it from the pc dimer.

After 72 h, the reaction was stopped and the solid was placed in a Soxhlet extractor and washed for > 24 h each with acetone and methanol to remove impurities. The crude green phthalocyanine fraction, composed of **1** and **2**, was extracted with chloroform until the extract in the extractor thimble was nearly colorless. The crude yield was about 300 mg. After gel-permeation chromatography (GPC) and HPLC, 98% pure **2** (based on the HPLC chromatography data) with a yield of 12% (from the limiting agent of tetracyanobenzene) was obtained. Our attempts at forming the side-by-side pc dimer were similar to the procedure of Lelievre's work [16], although the yield from the limiting agent in his report was 2.4%. The main differences in our procedure were pre-heating the bisdiiminoisoindoline (**8**) in DMAE before adding the other ingredients, and carrying out the entire reaction under a blanket of ammonia gas. Kobayashi's group [33] reported a 12% yield for the synthesis of his dinucleating pc ligand, non-metalated, by statistical synthesis in DMA, and about 8% each for the Co_2 and Zn_2 metalated analogs of **2**.

Purification of 1 and 2

Gel permeation chromatography (using BioBeads SX1, MW exclusion 600-14,000 amu) using toluene as

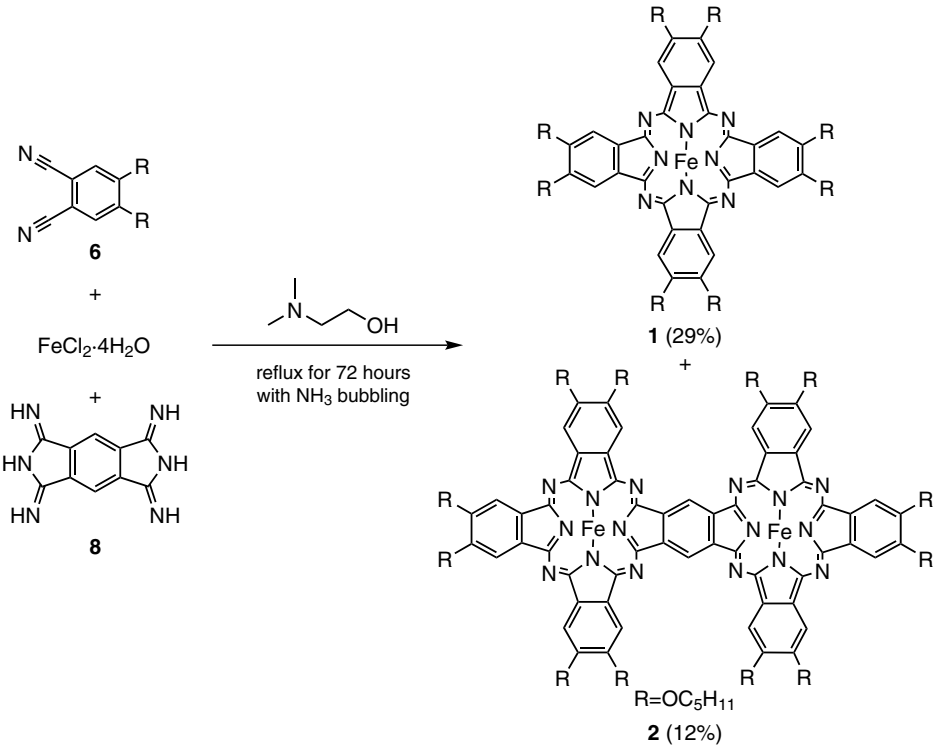

Scheme 2. Synthesis of **1** and **2**

eluent was used to enrich the fraction of dimer in the crude phthalocyanine material. The beads were swollen in toluene and packed into a chromatography column. After passage of the crude phthalocyanine material through the column, the first fraction was darker green and this (about 1/3 of the crude material) was the fraction used for HPLC purification. It consisted of about 50% **1** and 50% **2**. The second fraction coming out the column was bright green and consisted almost entirely of pc monomer (**1**, 96% purity before HPLC).

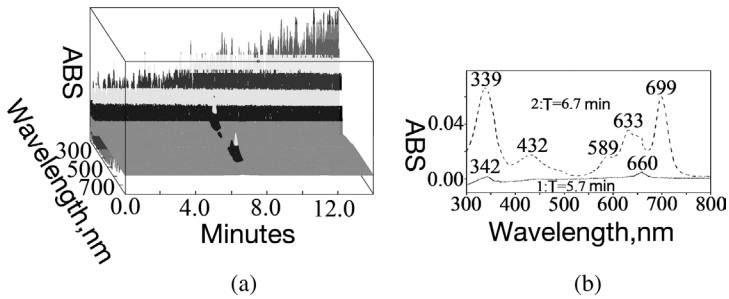

Fig. 2. HPLC chromatogram of **2** (silica column, 2% py in $CHCl_3$). Solid line in (b) is the UV-vis spectrum at the retention time of 5.7 min which was proved to be **1**, and dashed line is UV-vis spectrum at the retention time of 6.7 min which was proved to be **2**

HPLC separation was conducted using a semi-prep column of normal phase SiO_2 and an isocratic eluent of 2% pyridine in chloroform. Two major bands were present in the crude material, both with intense absorbance spectra characteristic of phthalocyanines, and the later band showing multiple peaks consistent with a dimeric pc. This band was assigned as the dimer, and the mass spectra of the purified fractions later confirmed the assumption. Compounds **2** (Fig. 2a) and **1** (Fig. S2, see the Supplementary material) were obtained in > 98% purity, as estimated by analytical HPLC. The process is reasonably scalable; a total of 130 mg of **1** and 120 mg of **2** were eventually isolated and purified.

Mass spectra

Phthalocyanines are often ionized by methods such as FAB, electrospray, and MALDI. According to the report of Freas [38], the macrocyclic backbone of phthalocyanine is difficult to fragment, but substituted phthalocyanines are fragile to the FAB ionization process, and sometimes the molecular peak is nowhere to be found. Based on the work of Lelievre [16], FAB usually breaks an alkyloxy chain of the main frame of the phthalocyanine during the ionization process. MALDI is a soft ionization technique used especially for fragile molecules. MALDI can measure the *m/z* of a molecule with molecular weight up to 10,000 Da [39–42] and it proved a reliable analytical method for **1** and **2**.

Compound **1** gave a strong peak at a *m/z* value of 1257.43 (theo. $[M + H]^+$ 1257.99), and the phthalocyanine dimer **2** gave intact singly charged ions, at a *m/z* value of 2092.79 (theo. $[M + H]^+$ 2092.21). The error of MALDI measurements is 0.1%, therefore for molecule **2**, a 2 dalton deviation would be acceptable. In many of the mass spectra, *m/z* peaks corresponding to ammonia adducts were observed. After HPLC purification, *m/z*

peaks corresponding to pyridine adducts were found for both **1** and **2**.

Even in HPLC purified **2**, which was 98% pure as assayed by HPLC peak integration, a strong MALDI peak of **1** or its pyridine coordination product was still present. The use of MALDI for quantitative analysis is limited [43–45]. The absolute intensity of the MALDI signal depends on the laser power, the matrix crystallization conditions, the ease of ionization of each compound, and the point-to-point repeatability. Because purified **2** contained only about 2% **1**, we think that **1** is much easier to ionize than **2**.

An *m/z* peak which equaled twice the molecular weight of the iron phthalocyanine monomer was always found in MALDI or FAB (see Fig. S6 in Supplementary material). Since several groups [11, 46, 47] have reported stacked metal pc dimers bonded *via* metal-metal bonds, we believe those peaks may correspond to the Fe-Fe bonded stacked phthalocyanine dimers; it is also possible the pc rings could dimerize during the MS ionization process. We see no evidence of this dimer species in the HPLC of **1**.

UV-vis titration of 1 and 2 with pyridine

Results. Pure **1** (99%) and **2** (98%) fractions were analyzed by UV-vis measurements. Their UV-vis spectra did not show the characteristic pc features. For example, the Q-band of both compounds was unusually weak. The MALDI spectra of these materials showed py-coordinated pcs were present, as described in the previous section. Because of the axial coordination capabilities of **1** and **2**, we thought the abnormal UV-vis results were from pyridine coordination. Pyridine titration experiments were performed on **1** and **2** (Fig. 3). First, the pyridine residue was removed from HPLC-purified **1** and **2** under high vacuum. Then, pyridine was injected into chloroform solutions of **1** and **2**. Since the maximum volume change due to the addition of pyridine was only 6%, the concentrations of the pcs were considered to be constant. After the titration experiments, two separate experiments were carried out where pyridine was used as the solvent so that very high concentration of pyridine was achieved. Detailed data can be seen in the Supplementary material.

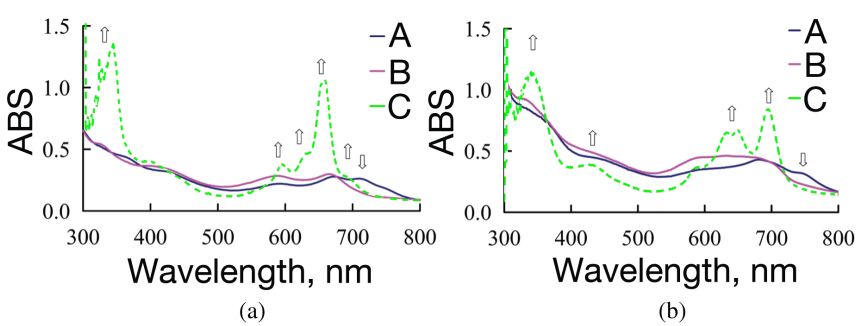

Fig. 3. UV-vis: pyridine titration. The arrows indicate the direction the spectra change when pyridine concentration is increased. (a): **1**(A: **1** in $CHCl_3$, B: 30.1:1 py/**1** in $CHCl_3$, C: **1** in py); (b): **2**(A: **2** in $CHCl_3$, B: 181:1 py/**2** in $CHCl_3$, C: **2** in pyridine. [**1**] = 6.4 × 10^{-3} M, [**2**] = 3.1 × 10^{-3} M)

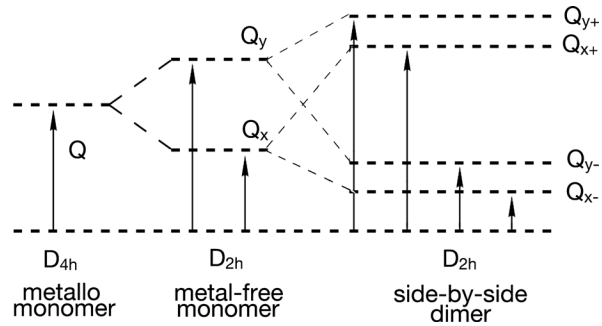

Fig. 4. Schematic diagram of electronic transitions of phthalocyanine [51]

Discussion of UV-vis spectra of 1. As illustrated in Fig. 4, in the metal-free pc monomer, the symmetry is lowered to D_{2h} from the D_{4h} symmetry of the metallo pc monomer because of the asymmetrical binding of the two H atoms. The excited state is split into two states termed Q_x and Q_y. These then are the two principal absorptions in the mononuclear species [48–51].

Because of the coordination capability of pyridine to iron, one or two pyridine molecules could ligate to **1**. For molecule **2**, one, two, three or four pyridines could ligate. Pc molecules have large aromatic systems and their intermolecular π-π interactions are strong, so π-stacking and aggregation are common. These two factors play important roles in the changes of the UV-vis spectra of pc molecules. Regular pc molecules tend to have cofacial aggregation, as shown in phase A in Scheme 3 [13, 35, 52, 53]. When pc molecules aggregate, the Q-band peak tends to shrink and broaden and its shoulder peaks increase in intensity [15, 54]. In Dominguez's work, the UV-vis spectra of a poly(ethyleneoxide)-capped phthalocyanine in $CHCl_3$, which physically can only aggregate to a dimer, were taken. One of the clearest findings was that the Q-bands shrank drastically when the concentration of the pc was increased. At the same time, the intensity of the shoulder peaks increased. Their results showed that for a cofacial dimer species, the Q-band was much smaller than usual, comparable in intensity to the shoulder peaks.

In the case of our experiments, the concentration of pc remained constant and the concentration of pyridine changed. With excess pyridine, the aggregates of **1** should break up and **1**-$(py)_2$ should be formed in the end. Five possible phases (A′, A, B′, B and C) are presented in Scheme 3. Three of them (A, B, C) correspond to the UV-vis spectra at the three indicated stages (A, B, C) of Fig. 3a.

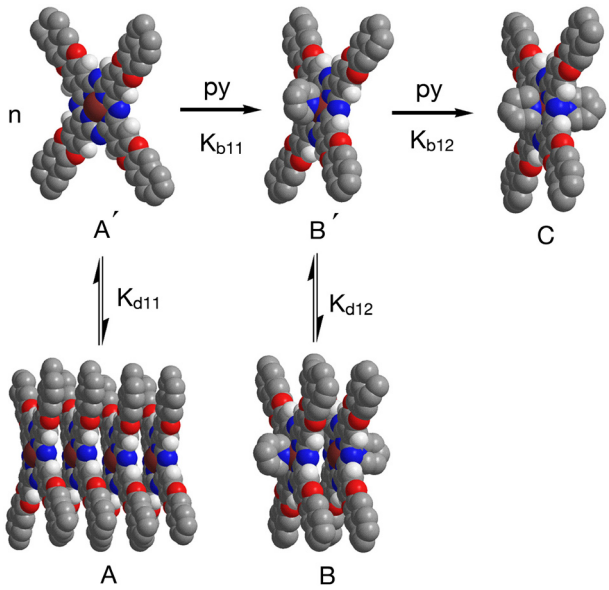

Scheme 3. Reactions of **1** with pyridine

At the very beginning of the titration process a very broad and suppressed Q-band was seen, and the Soret band was suppressed too. These features are consistent with extensive cofacial aggregation of **1** (stage A of Fig. 3a) [35]. Because of the aggregation, the Q-band and the shoulder peaks (673, 586 nm) were very broad.

As pyridine was added to the solution, the coordination of pyridine to the central Fe atom of **1** broke the aggregation and **1**-py was formed (phase B′ in Fig. 3a). Aggregation (K_{d12}) could occur to form cofacial dimers (phase B in Scheme 3). The new Q-band and shoulder peak (668 nm and 585 nm) are assigned to this cofacial dimer. The UV-vis spectrum of phase B (stage B in Fig. 3a) showed broad peaks at 681 nm and 589 nm, and the intensity of the Soret band (330 nm) was very small as expected for a partially aggregated species.

At high pyridine concentrations, a intense Q-band (660 nm, log ε = 4.12) was finally observed. Two shoulder peaks were found at 631 nm and 569 nm, which are assigned as vibronic excitation [55–57]. A strong Soret band (343 nm, log ε = 4.22) was also found. J. Janczak has measured the absorption coefficient for FePc(pyrazine)$_2$ in 1-chloronaphthalene (662 nm, log ε = 6.71) which is significantly larger than our observed extinction coefficient; however, this involved a different axial ligand [57]. MJ Stillman also measured the absorption coefficient for FePc(py)$_2$ in DMSO (667 nm, log ε = 4.88) [58]. Comparing this absorption coefficient with that of molecule **1** in pyridine (660 nm, log ε = 4.12), the difference is not substantial considering a different solvent was used. After a large excess of pyridine was added, the equilibrium in the solution shifted to form a six-coordinated Fe complex with both axial positions occupied by pyridine (**1**-(py)$_2$, phase C in Scheme 3). This broke up the cofacial dimer and isolated **1**-(py)$_2$ was formed. The shoulder at 700 nm was assigned as residual cofacial aggregation [35]. This assignment was supported by the fact that the intensity of the peak at 700 nm in Fig. S8a (see the Supplementary material) decreased when the concentration of pyridine increased. The existence of the peak at 700 nm, indicated that not all the molecules of **1** were present as **1**-(py)$_2$, even when neat pyridine was used as the solvent.

There are two kinds of charge transfer peaks normally seen in the UV-vis spectra of FePcs: one caused by MLCT (metal-ligand charge transfer) and for alkoxyl-substituted pcs, one caused by oxygen-to-pc(π*) [20, 60] charge transfer. In supplementary Fig. S8a, the peak at 425 nm remains at the same wavelength for the whole titration process, so it is unlikely to be caused by MLCT. Therefore, the peak at 425 nm was assigned to the oxygen-to-pc(π*) charge transfer [17, 61]. Since the peak at 402 nm became bigger when the concentration of pyridine increased, it was reasonable to assign this peak as the MLCT peak.

Discussion of UV-vis spectra of 2. As shown in previous reports on side-by-side metal-free [62–64] and metallophthalocyanine dimers [16, 33, 63, 65, 66] the Q-bands of side-by-side pc dimers are blue-shifted compared to the corresponding monomers. An exciton coupling model explains the blue shift (Fig. 4). In the side-by-side dimer, there are transition moments of the two excited states (Q_x, Q_y) that couple, in and out-of-phase, between the two halves of the binuclear molecule. In D_{2h} symmetry of side-by-side phthalocyanine dimer, the Q_x and Q_y states (as in D_{2h} symmetry of metal free phthlocyanine monomer) split and the coupling result in a pair of nondegenerate in-phase higher energy combinations (Q_{y+}, Q_{x+}) and a pair of lower energy out-of-phase combinations (Q_{y-}, Q_{x-}) (Fig. 4) [51]. The lower energy combinations (Q_{y-}, Q_{x-}) give the red shifted Q-band.

Again, axial coordination and co-facial aggregation play important roles in the UV-vis spectra of **2**. Five possible phases (A′, A, B′, B and C) are presented in Scheme 4. Three of them (A, B, C) are assigned to the UV-vis spectra at three stages (A, B, C) in Fig. 3b. In the

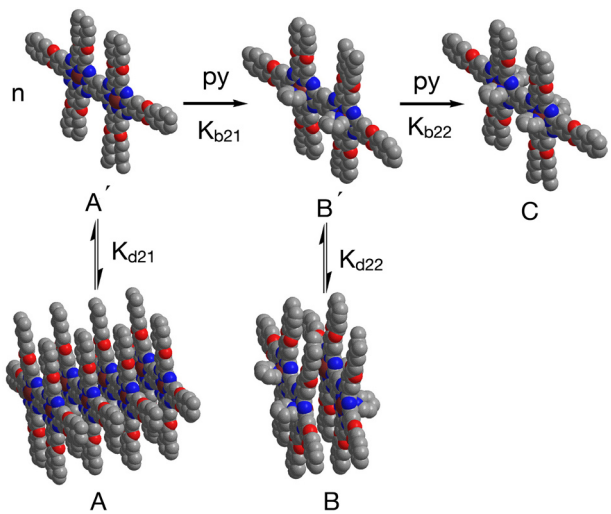

Scheme 4. Reaction schemes of **2** with pyridine

presence of excess pyridine, the UV-vis spectra indicate that the aggregation of **2** is broken and a highly coordinated species (**2**-$(py)_4$ and/or **2**-$(py)_3$) is formed.

When no pyridine is present, the UV-vis spectrum of **2** (stage A in Fig. 3b) shows a broadened Q-band (683 nm) and a shoulder (582 nm). The low-energy peak (745 nm) due to cofacial aggregation was fairly strong, and the Soret band (370 nm) was weak. This spectrum corresponds to the aggregated phase A in Scheme 4.

As pyridine is added, these aggregates are broken up as mono, bi, or tripyridyl-**2** molecules are formed by coordination to the two Fe atoms (phase B in Scheme 4). Some aggregation appears to persist until a very high concentration of pyridine is reached. Phase B of Scheme 4 shows *cis*-**2** (Fe(py)-Fe(py)) aggregates. However, even for a two-pyridine addition product, there also could be *trans*-**2**(Fe(py)-Fe(py)) or **2**(Fe-Fe$(py)_2$), and these species could form different types of aggregates due to π-π stacking interactions. The mixture of multiple coordination types and aggregation states gives a very broad Q-band at 684 nm and a shoulder (589 nm) (stage B in Fig. 3b). The low energy peak at 745 nm is reduced in intensity, but the Soret band at 335 nm was still depressed due to aggregation.

At very high pyridine concentrations, tri- or tetrapyridyl-**2** molecules with spectroscopic characteristics of isolated pc dimers are observed. When neat pyridine was used as the solvent, the Q-band and Soret band reached the highest intensity (phase C in Fig. 3b). The signatures for disaggregation in phase C include: an intense Q-band (696 nm, log ε = 4.57), loss of the low-energy band at 745 nm, and a strong Soret band (344 nm, log ε = 4.70). Several sharp vibronic shoulder peaks were also visible (651 nm, 634 nm and 589 nm). The ligand-metal charge transfer peak was not visible. It could be blue-shifted and buried under the peak at 420 nm. The peak at 420 nm was assigned as the oxygen-to-π* charge-transfer band of **2**. This assignment is supported by the fact that (Figs S8a,b) the peaks at 420 nm remain at the same position regardless of the change of the concentration of pyridine.

NMR

Previous studies on phthalocyanine monomer and dimer molecules have had great difficulties to obtain well resolved NMR spectra [21, 67–69] even for soluble pc monomers and dimers which have side chains [54, 70, 71]. Because phthalocyanine molecules are big (> 2 nm) and rigid, they have limited solubility and tend to aggregate in solution, which decreases their tumbling rate. Their aromatic cores have relatively long proton relaxation times. This behavior is also observed for metallo pc molecules [27, 72, 73]. For typical NMR measurements on pcs, low concentrations [27, 54, 73] and special solvents, such as CS_2 [16] or toluene [73], were used to depress aggregation.

The NMR spectra of **1** and **2** were obtained in $CDCl_3$ but both spectra appeared to contain multiple species as shown by the number and broadened envelopes of peaks. In view of the UV-vis results, both phthalocyanines are expected to be partially aggregated under these conditions, and the aggregates are high enough in molecular weight to cause NMR peak broadening due to slow tumbling rates. A trace amount of pyridine was present due to its use in the HPLC eluent, so one or two pyridine molecules could ligate to **1** and make mixtures of **1**-py and **1**-$(py)_2$. For the dimeric phthalocyanine **2**, the mixture could include **2**-py, **2**-$(py)_2$, **2**-$(py)_3$ and even **2**-$(py)_4$. As seen in Fig. S10, because of the existence of multiple coordination compounds, some strongly aggregated, and multiple isomers of these compounds, their NMR spectra were broad and very complicated. Addition of about four drops of py-d_5 clarified the NMR spectra greatly for both **1** and **2**. Figures 5 and 6 show NMR spectra of **1** and **2** in $CDCl_3$/py. With addition of excess pyridine, all the coordination positions were occupied and single coordination compounds were formed. In the NMR tube reaction, py-d_5 was used. At this point, the NMR spectra of **1** and **2** were greatly simplified.

As shown in Table 1, the chemical shift of the phenyl proton of **1** (H_a) appears as a slightly broadened singlet at 8.66 ppm, a value which is typical for aromatic protons on a phthalocyanine core. The chemical shift of the "bridging" phenyl proton of **2** (H_g) is 9.74 ppm, which is reasonable considering the influence of the two 18-member aromatic rings. The other phenyl protons in compound **2** (H_h, H_g and H_i) had chemical shift values of 8.72 ppm, 8.69 ppm and 8.68 ppm, respectively. Strong residual pyridine peaks at (8.50, 7.55, 7.12 ppm) are visible in

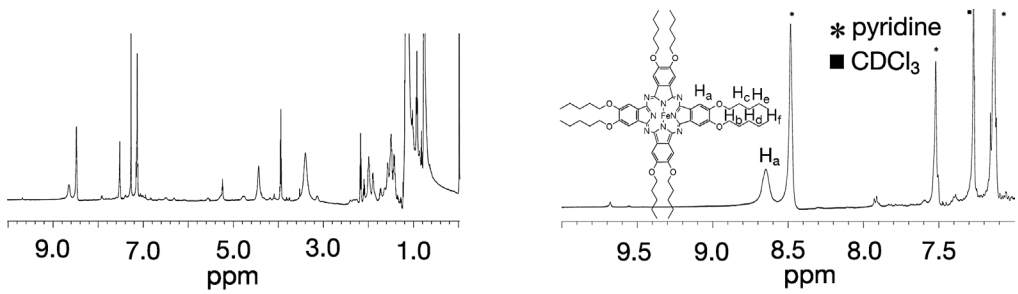

Fig. 5. NMR spectra of **1** in $CDCl_3$ with py-d_5. (a) full field (b) low field region

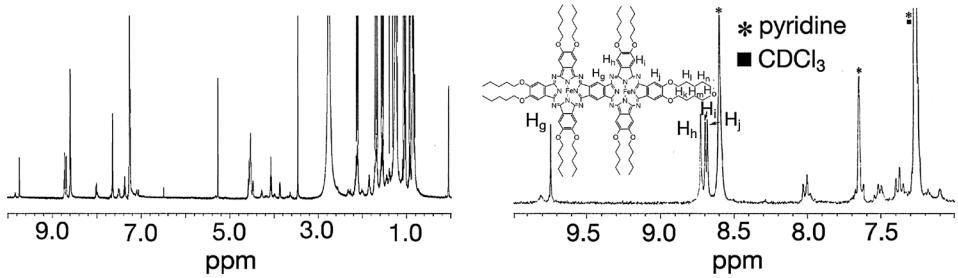

(a) (b)

Fig. 6. NMR spectra of **2** in $CDCl_3$ with py-d_5

Table 1. Proton NMR assignment of **1** and **2**[a]

1	H_a	H_b	H_c	H_d,H_e	H_f
ppm	8.66 (4)	4.42 (8)	2.17 (8)	1.50 (16)	0.92 (12)
2	H_g	H_h	H_i	H_j	H_k
ppm	9.74 (3[b])	8.72 (4)	8.69 (4)	8.68 (4)	4.55-4.37 (24)
	H_l	H_m	H_n	H_o	
	2.12 (24)	1.70 (24)	1.53 (24)	1.03 (36)	

[a] The numbers in brackets are the integrated intensity values.
[b] The integration of Hg is discussed in the text.

the NMR of **1** with py-d_5 (Fig. 5b) and at (8.59, 7.64, 7.27 ppm) in the NMR of **2** with py-d_5 (Fig. 6b); they were identified by comparison to the reference data of pyridine in chloroform (8.62, 7.68, 7.29 ppm) [74]. No peaks were observed for coordinated pyridine because of the low quantity of protonated pyridine present in the samples. For compound **2**, some of the integrations could not be measured well. For example, the integration of H_g was 50% more than the theoretical value due to a small overlapping impurity peak. Several small peaks are clearly present in the aromatic region, which may indicate the presence of multiple coordination states or aggregation states in the sample. The CH_2O protons of the pentyloxy side chains appeared as clear triplets at 4.42 ppm and 4.46 ppm for **1** and **2**, respectively, and the peak positions and intensities for the rest of the pentyloxy chains were consistent with previous reports [16, 64, 75].

Electrochemistry

Electrochemical data were obtained with cyclic voltammetry (CV) and square-wave voltammetry (SW) in a nitrogen-filled dry box with electrical feedthroughs. The working electrode was a Pt disk, and we found it necessary to polish the electrode before each run. In the cyclic voltammetry experiment, the applied potential is systematically swept over a desired range while measuring current at the working electrode. In the square-wave voltammetry experiment, the voltage is held at a starting value and a square-wave pattern is used to jump up to sequentially higher voltages, each time returning to the starting value. The current at the working electrode is recorded at end of every cycle and plotted against the potential change. The reduction or oxidation peak can appear as a peak or trough, depending on the sweep direction. All the experiments were kept at initial potential for several seconds before starting to scan, and all the SW voltammograms were taken with 5 sec of quiet time.

Since the electrochemistry data of **1** and **2** are complicated and interaction with pyridine also shifts their redox potentials, the data will be presented and discussed in three subsections. First, the cyclic voltammetry and square-wave voltammetry data of **1** and **2** are presented. Second, the literature data of pc ring and central metal redox behaviors are summarized, along with discussion of the influence of solvent and ligands on the redox potentials of metallophthalocyanines. Finally, the assignment of the redox waves in compounds **1** and **2** is discussed.

Electrochemistry results for 1 and 1-py. Electrochemical studies were done in methylene chloride. Without adding pyridine to **1**, the CV and SW spectra were not very clear or interpretable. Some typical CV and SW voltammograms of **1** are shown in the Supplementary material (Figs S11–S13). In order to break up aggregation of the phthalocyanine rings, 30 mM pyridine was added to 1.0 mM **1**; under these conditions, the main species is the cofacially aggregated dimer of **1**-py. Figure 7 shows the resulting SW voltammogram. The cathodic sweep showed peaks at 1.29, 0.71, -0.90, and -1.21 V, and the anodic sweep showed peaks at 0.86, 0.68, 0.19, -0.41, -0.75, and -0.88 V.

Known electrochemistry of phthalocyanine monomers. For Fe(II)Pc, the first ring oxidation occurs at potentials from 0.74 to 1.22 V, depending on the solvent and whether there is a coordinating ligand present; the first ring reduction occurs at potentials ranging from -1.1 to -1.5 V and is also affected by the presence of coordinating ligands [76, 77]. As seen in Table 2, oxidation of the central Fe(II) in FePc is observed at potentials between 0.17 and 0.66 V, with more positive oxidation potentials observed in the presence of π-backbonding ligands such as pyridine. Reduction of Fe(II) in Fe(Pc) is observed at potentials around -0.86 to -1.07 V depending on the chelation ability of solvents and eletrolytes.

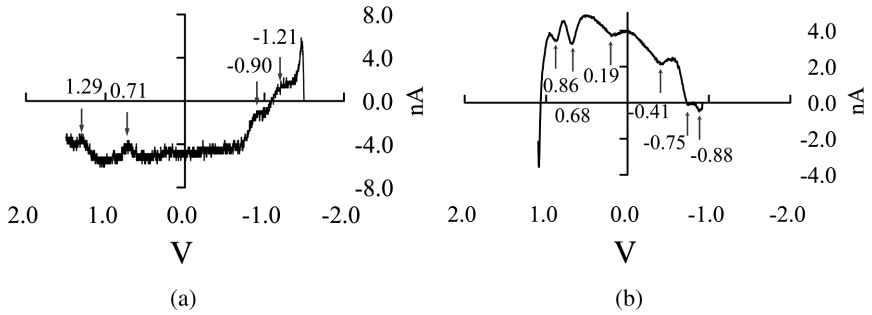

Fig. 7. Square-wave voltammograms of **1** in CH_2Cl_2 with 1.00 mM **1**, 30.0 mM pyridine (a: anodic scan and b: cathodic scan)

Table 2. Redox potentials of FePc complexes[a]

Solvent	electrolyte	Fe^{III}/Fe^{II}	Fe^{II}/Fe^{I}	First ring reduction
pyridine	TEAP[b]	0.66	-1.07	-1.316
	TEABr[c]		-1.05	-1.283
DMA	TEAP[b]	0.38	-0.55	-1.169
	TEABr[c]	0.17	-0.86	-1.194

[a] 0.0005 M FePc, V *vs.* SCE, [80]. [b] 0.1 M solution of TBAP (tetrabutylammonium perchlorate). [c] 0.1 M solution of TEABr (tetrabutylammonium bromide).

There are few reports of Fe-centered redox processes in non-coordinating solvents and in the absence of coordinating ligands. Wolberg and Manasson [78] reported the Fe^{III}/Fe^{II} redox potential for FePc in chloronapthalene at 0.19 V, and Campbell *et al.* [79] report a reduction potential of -0.95 V for the Fe^{II}/Fe^{I} process for Fe[*t*-BuPc] in CH_2Cl_2 (DCM).

Discussion of electrochemistry of 1 and 1-py. When compound **1** was studied by cyclic voltammetry or square-wave voltammetry, only weak or indistinct peaks were observed, even at mM concentrations. This is probably due to the aggregation of the pc molecules. The clearest voltammograms were measured when excess pyridine was added to the solution to form pyridine-coordinated **1**. According to the UV-vis titration results, for a 1 mM solution of **1** in the presence of 30 equivalents of pyridine the major species is the 1:1 complex **1**-py, which would mostly exist as a dimer.

The initial anodic SW sweep is shown in Fig. 7a. Peaks were observed at -1.21, -0.90, +0.71, and +1.29 V. The reduction wave at -1.21 V is assigned as the first reduction of the pc ring in **1**; this reduction occur at -1.27 V in the parent compound FePc (in pyridine solvent). The reduction at -0.90 V is assigned as the reduction of the Fe(II) in **1**; in the parent compound FePc this reduction was observed at -1.07 V in the presence of pyridine (the Fe reduction potential in FePc shifts to -0.55 V in a non-coordinating solvent, DMA). The first oxidation peak (0.71 V) in Fig. 7a was assigned to the oxidation of Fe^{II} in **1**-py, where the Fe(II) is stabilized by pyridine coordination. In prior work by Lever [80], the first oxidation potential of FePc occurred at 0.66 V in neat py; the assignment was confirmed by electron spin resonance (ESR) data. The 0.71 V process was electrochemically irreversible (no return wave in CV). The last oxidation wave at 1.29 V is assigned as the first ring oxidation of the pc ring in **1**; this ring oxidation was observed at 1.05–1.10 V in the parent compound FePc in pyridine solvent [78].

When Fe^{III}Pc-py is formed, the coordinated pyridine falls off [80]. The resulting mixture of py-coordinated **1** and uncoordinated **1** gives the complex return wave in Fig. 7b, which shows peaks at 0.86, 0.68, 0.19, -0.41, -0.75, and -0.88 V.

The oxidation peak at 0.86 V was assigned to the first ring oxidation of py-free **1**. The peak at 0.68 V is assigned to the oxidation of the Fe(II) in **1**-py (seen at 0.71 V in the cathodic sweep). The weak peak at 0.19 V in Fig. 7a is assigned to oxidation of the Fe(II) in py-free **1**, which is the same as the potential for oxidation of Fe(II) in FePc in chloronapthalene, 0.19 V [78]. Comparing the Fe^{III}/Fe^{II} reduction potentials of py-coordinated (0.71 V) and py-free (0.19 V) **1**, we could see that Fe^{II}Pc was harder to oxidize in py-containing solution, presumably due to the back-bonding interactions between the Fe(II) center and the pyridine pi system. The reduction wave at -0.41 V is assigned as the first reduction of Fe^{II} in py-free **1**. In the voltammograms of **1** (Fig. 7a,b), the separation between the first Fe oxidation and first Fe reduction was smaller for py-free **1** (oxidation 0.19, reduction -0.41, separation of 0.60 V) than for py-coordinated **1** (oxidation 0.71 V, reduction -0.90 V, separation of 1.61 V). The reported separation [80] between Fe(II) oxidation and reduction potentials in FePc ranges from 0.5–1.2 V for weakly coordinating solvents but rises to 1.7–1.9 V in neat pyridine. The second reduction peak for compound **1** at -0.75 V is tentatively assigned as the first ring reduction of py-free **1**. The final reduction peak (-0.88 V) was assigned as the reduction of the Fe(II) in **1-**py, seen at -0.90 V in the cathodic sweep. Thus the pyridine-free **1** is associated with redox peaks at 0.86 V, 0.19 V, -0.40 V and -0.75 V. In cyclic voltammograms of py-free **1**, Fig. S12 (Supplementary material), although the capacitive background was high, weak peaks at 0.763 V, 0.145 V, -0.50 V and -0.84 V were identified. All the peak assignments are listed in Table 3.

Table 3. Electrochemical data for **1** ($E_{1/2}$/V[a])

	Couple	$E_{1/2}$/V
1-py	$Fe^{III}Pc(-1)/Fe^{III}Pc(-2)$	1.29
	$Fe^{III}Pc(-2)/Fe^{II}Pc(-2)$	0.71
	$Fe^{II}Pc(-2)/Fe^{I}Pc(-2)$	-0.90
	$Fe^{I}Pc(-2)/Fe^{I}Pc(-3)$	-1.21
1	$Fe^{III}Pc(-1)/Fe^{III}Pc(-2)$	0.86
	$Fe^{III}Pc(-2)/Fe^{II}Pc(-2)$	0.19
	$Fe^{II}Pc(-2)/Fe^{I}Pc(-2)$	-0.40
	$Fe^{I}Pc(-2)/Fe^{I}Pc(-3)$	-0.75

[a] Potentials are reported with respect to the SCE couple.

Electrochemistry results for 2 and 2-py. In the absence of pyridine, the CV and SW spectra of **2** were not very clear or interpretable. Some typical CV and SW voltammograms of **2** are shown in the Supplementary material. Pyridine was added to **2** to break up the aggregation. Figure 8 shows the SW voltammogram of 1.2 mM **2** in the presence of 857 mM pyridine. The spectrum shows peaks assigned as py-coordinated **2** (see Discussion of electrochemistry of **2** and **2**-py section hereafter) in the cathodic (1.45, 1.20, 0.84, -0.67, -0.89, -1.23, -1.28 V) and anodic (1.16, 0.93, 0.52, -0.43, -0.65, -0.90, -1.21 V) scans.

Known electrochemistry of phthalocyanine dimers. As seen in Table 4, Kobayashi observed six redox processes for a binuclear pc (with six solubilizing neopentyloxy side chains) whose aromatic core is nearly identical to that of **2** [33]. This compound, which lacks a redox active metal, showed two quasi-reversible ring oxidations at 0.66 and 0.41 V *vs.* SCE. and four quasi-reversible ring reductions (-0.85, -1.11, -1.45, and -1.70 V *vs*. SCE) in the non-coordinating solvent dichlorobenzene. The ring oxidations are separated by about 250 mV, and the ring reductions form two pairs with separations of about 250 mV each. The first ring reduction couple is shifted positively by about 300 mV relative to the value for the analogous monomeric phthalocyanine, and the first ring oxidation couple is shifted negatively by about 70 mV.

The CV and DPV of $(CoPc)_2$ were also obtained [33]. Because of cobalt's redox activity, the voltammograms were more complex than for $(ZnPc)_2$. In dichlorobenzene solution, the splitting of the two successive Co^{II}/Co^{I} couples was fairly large (about 500 mV), and the ratio of area of the peaks deviated from the theoretical ratio. The authors assigned four redox couples to stepwise reductions of the two phthalocyanine units in $(CoPc)_2$. The redox potentials for the first metal oxidation in CoPc and $[CoPc]_2$ are virtually identical.

As the influence of pyridine on the redox potentials of iron phthalocyanine dimers has not been established, we used the data of the influence of pyridine on **1** to help assign our electrochemistry data for **2**.

Discussion of electrochemistry of 2 and 2-py. The cyclic voltammograms and square wave voltammograms of pure **2** were weak and complicated, but after addition of about 700 equivalents of pyridine, the voltammograms became clearer. According to our UV-vis experiment, at these concentrations, **2** was about halfway occupied by pyridine to form **2**-$(py)_2$, which still could aggregate to form cofacial dimers.

In the cathodic square-wave scan, three oxidation waves and four reduction waves were observed (at 1.45, 1.20, 0.84, -0.67, -0.89, -1.23, and -1.28 V *vs*. SCE, Fig. 8a and Table 5). The anodic scan showed most of the expected return waves along with two new waves (at 1.16, 0.93, 0.52 (new), -0.43 (new), -0.65, -0.90, and -1.21 V, Fig. 8b and Table 5). We think the new peaks arise due to loss of pyridine coordinated to **2** during the oxidative preparation, which allows peaks that belong to redox processes of py-free **2** to appear. We assumed that

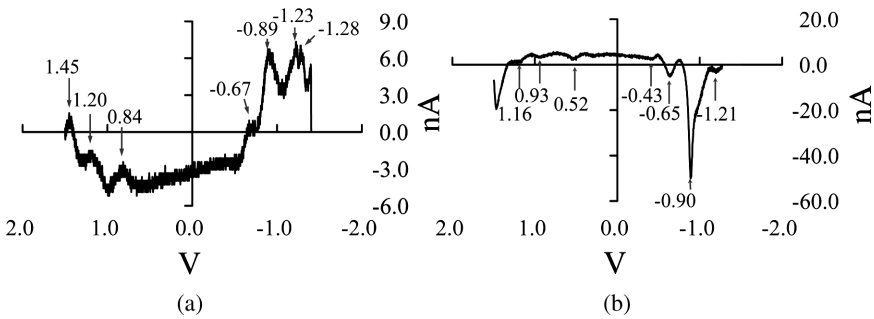

Fig. 8. Square-wave voltammograms of **2** in CH_2Cl_2 with 1.20 mM **2**, 857 mM pyridine (a: anodic scan and b: cathodic scan)

Table 4. Redox potentials of side-by-side pc dimer $(ZnPc)_2$ complexes[a]

Second ring oxidation	First ring oxidation	First ring reduction	Second ring reduction	Third ring reduction	Fourth ring reduction
0.66	0.41	-0.85	-1.11	-1.45	-1.70

[a] 0.002 M pc dimer in 0.1–0.3 M solution of TBAP in dichlorobenzene, in V *vs.* SCE [33].

Table 5. Electrochemical data for **2** ($E_{1/2}$/V[a])

	Couple	$E_{1/2}$/V
2-py$_2$	$[Fe^{II}Pc(-1)Fe^{III}Pc(-1)]/[Fe^{II}Pc(-1)Fe^{III}Pc(-2)]$	1.45
	$[Fe^{II}Pc(-1)Fe^{III}Pc(-2)]/[Fe^{II}Pc(-2)Fe^{III}Pc(-2)]$	1.20
	$[Fe^{II}Pc(-2)Fe^{III}Pc(-2)]/[Fe^{II}Pc(-2)]_2$	0.84
	$[Fe^{II}Pc(-2)]_2/[Fe^{II}Pc(-2)Fe^{I}Pc(-2)]$	-0.62
	$[Fe^{II}Pc(-2)Fe^{I}Pc(-2)]/[Fe^{I}Pc(-2)]_2$	-0.89
	$[Fe^{I}Pc(-2)]_2/[Fe^{I}Pc(-3)Fe^{I}Pc(-2)]$	-0.89
	$[Fe^{I}Pc(-3)Fe^{I}Pc(-2)]/[Fe^{I}Pc(-3)]_2$	-1.23
	$[Fe^{I}Pc(-3)]_2/[Fe^{I}Pc(-3)Fe^{I}Pc(-4)]$	-1.28
2	$[Fe^{III}Pc(-1)]_2/[Fe^{II}Pc(-1)Fe^{III}Pc(-1)]$	1.46
	$[Fe^{II}Pc(-1)Fe^{III}Pc(-1)]/[Fe^{II}Pc(-1)Fe^{III}Pc(-2)]$	1.16
	$[Fe^{II}Pc(-1)Fe^{III}Pc(-2)]/[Fe^{II}Pc(-2)Fe^{III}Pc(-2)]$	0.93
	$[Fe^{II}Pc(-2)Fe^{III}Pc(-2)]/[Fe^{II}Pc(-2)]_2$	0.52
	$[Fe^{II}Pc(-2)]_2/[Fe^{II}Pc(-2)Fe^{I}Pc(-2)]$	-0.43
	$[Fe^{II}Pc(-2)Fe^{I}Pc(-2)]/[Fe^{I}Pc(-2)]_2$	-0.65
	$[Fe^{I}Pc(-2)]_2/[Fe^{I}Pc(-3)Fe^{I}Pc(-2)]$	-0.65
	$[Fe^{I}Pc(-3)Fe^{I}Pc(-2)]/[Fe^{I}Pc(-3)]_2$	-0.99
	$[Fe^{I}Pc(-3)]_2/[Fe^{I}Pc(-3)Fe^{I}Pc(-4)]$	-1.21

[a] Potentials are reported with respect to the SCE couple.

the shifts in potential between FePc and $(FePc)_2$ will be similar to the corresponding shifts in potential for known CoPc and $(CoPc)_2$ redox transitions and that the influence of pyridine on the electrochemistry of $(FePc)_2$ will be similar to that of FePc.

Since we assigned 0.71 V to py-coordinated $Fe^{III}Pc(-2)/Fe^{II}Pc(-2)$ in **1** and 0.19 V to the same transition in py-free **1**, the anodic 0.84 V wave (observed at 0.93 V in the cathodic scan) of compound **2** probably belongs to the first Fe^{II} oxidation ($[Fe^{II}Pc(-2)Fe^{III}Pc(-2)]/[Fe^{II}Pc(-2)]_2$) of py-coordinated **2** and the new peak at 0.52 V to the first Fe^{II} oxidation of py-free **2**.

For compound **1**-py, the first ring oxidation was observed at 1.29 V; a shift of 70 mV negatively should give a peak around 1.22 V. There are two possible assignments, but since the second ring oxidation should be about 250 mV more positive than the first ring oxidation, the peaks at 1.20 and 1.45 V was assigned to the first and second pc ring oxidation of py-coordinated **2**. Likewise, py-free **1** showed its first ring oxidation at 0.86 V; a 70 mV negatively should give a peak around 0.79 V. The oxidation peak at 1.46 V for py-free **2** is assigned to the second Fe^{III}/Fe^{II} oxidation. The peaks at 0.93 V and 1.16 V were accordingly assigned to the first and second ring oxidations of py-free **2**.

From the results of Lever [80], the separation between the first Fe^{II} oxidation and reduction of a py-coordinated FePc monomer was about 1.73 V. This observation made us chose -0.65 V as the first Fe^{II} reduction for py-coordinated **2**. Because the py-coordinated FePc monomer had a larger separation between the first Fe^{II} oxidation and reduction than py-free FePc [80], the peak at -0.43 V was assigned to the first Fe^{II}/Fe^{I} reduction of py-free **2**.

Similarly, the peak at -0.89 V in the py-coordinated **2** was about twice the size of other peaks for py-coordinated **2**. This peak was assigned to the overlapping couples of $[Fe^{II}Pc(-2)Fe^{I}Pc(-2)]/[Fe^{I}Pc(-2)]_2$ and $[Fe^{I}Pc(-2)]_2/[Fe^{I}Pc(-3)Fe^{I}Pc(-2)]$ of the py-coordinated **2**. The reduction potentials of the two steps were expected to be very close and we could not tell the sequence of these two steps. Since the peak at -0.65 V of py-free **2** was also twice the size of the other peaks, it was treated as a two electron addition process, composed of adding one electron to the metal and the other electron to the ring. Therefore, the -0.65 V was assigned to the $[Fe^{II}Pc(-2)Fe^{I}Pc(-2)]/[Fe^{I}Pc(-2)]$ and $[Fe^{I}Pc(-2)]_2/[Fe^{I}Pc(-3)Fe^{I}Pc(-2)]$ of py-free **2**.

The peaks at -1.23 V and -1.28 V were assigned as the consecutive reductions on the pc rings of py-coordinated **2** since it was not enough to reduce Fe^{I} to Fe^{0}. Similarly, the -0.99 V and -1.21 V were assigned to the consecutive reductions on the pc rings of py-free **2**. The trough at -0.90 V was much bigger than the others and we are not sure of the cause. In Kobayashi's paper [33], the sizes of the peaks were also not proportional the number of the electron exchanges.

As discussed above, both **1**-(py) and **2**-$(py)_2$ could lose their axial pyridine ligands if the Fe^{II} was oxidized to Fe^{III}. Figure 7b shows redox waves of both py-free and py-coordinated **1** molecules, which confirmed partial dissociation of py-FePc during the 5 sec of electrolysis at 1.5 V. The same process happens for py-coordinated **2** during the 5 sec of cathodic electrolysis. In Fig. S13 (Supplementary material), peaks of py-free **2** at 0.62 V and 0.92 V were close to the first two oxidation peaks (0.52 V, 0.92 V) in the cathodic scan of py-coordinated **2** (Fig. 8b). The first reduction peak of py-free **2** (-0.64 V) was not very close to that (-0.43 V) of the cathodic scan of py-coordinated **2** (Fig. 8b). The difference between the cathodic voltammograms of py-coordinated **1** and py-coordinated **2** was that in Fig. 7b a mixture of py-free and py-coordinated **1** can be seen, while in Fig. 8b, py-free **2** appears to be the major species present.

Mixed-valence properties of the side-by-side iron(pc) dimer 2. Electrochemical data can give information about the stability of mixed-valence compounds which is a key metric for use in molecular QCA. Scheme 5 shows two potential formation reactions, oxidation I and reduction II, for mixed-valence compounds based on **2**. Using Equation III, where the ΔE is the difference in redox potentials for the two compounds shown in each formation reaction, we can calculate comproportionation constants (K_c at 20 °C) listed in Table 6. Here the two solvent

$$[Fe^{II}Pc(-1)Fe^{III}Pc(-2)] + [Fe^{II}Pc(-2)]_2 \rightarrow 2[Fe^{II}Pc(-2)Fe^{III}Pc(-2)] \quad (I)$$

$$[Fe^{II}Pc(-2)]_2 + [Fe^{I}Pc(-2)]_2 \rightarrow 2[Fe^{II}Pc(-2)Fe^{I}Pc(-2)] \quad (II)$$

$$\Delta E = \frac{RT}{F} \ln K_c \quad (III)$$

Scheme 5. Mixed-valence formation reactions of **2**

Table 6. Comproportionation data

Couple[a]	Solvent[b]	ΔE/V[c]	K_c[d]	K_d[e]	ΔG(Kj/mol)
I	A	0.41	1.1×10^7	9.1×10^{-8}	-39
I	B	0.36	1.5×10^6	6.4×10^{-7}	-35
II	A	0.22	6.1×10^3	1.7×10^{-4}	-21
II	B	0.26	3.0×10^4	3.4×10^{-5}	-25

[a] I, II correspond to couples I, II in Scheme 5. [b] A = CH_2Cl_2, B = 0.86 mM pyridine in CH_2Cl_2. [c] Mixed-valence splitting energy. [d] Comproportionation constant. [e] Discomproportionation constant, $1/K_c$.

environments were appointed as CH_2Cl_2 (environment A) and 0.86 mM pyridine in CH_2Cl_2 (environment B). In the CH_2Cl_2 environment the py-free **2** values were used and in the pyridine solution, **2**-py_2 data were used.

The comproportionation constant (K_c) of oxidation reaction I was over 1.6×10^6 in both solvents – 1.1×10^7 in pure DCM, and 1.6×10^6 in DCM with 0.86 mM pyridine. The difference is probably not significant given the difficulty of pinpointing the redox potentials. The K_{com} for $\mathbf{2}^+$ is comparable to the value for a well known, stable mixed-valence compound, the Creutz-Taube ion, ($[(NH_3)_5Ru\text{-}pz\text{-}Ru(NH_3)_5]^{5+}$, for which $K_{com} = 4 \times 10^6$) [19]. The comproportionation constant (K_c) for $\mathbf{2}^-$ (formed by reduction reaction II) was smaller, measuring 6.1×10^3 (DCM) and 3.0×10^4 (DCM/py).

Multiple attempts were made to electrolyze **2** in the presence of pyridine to form the oxidized mixed-valence species. Several attempts failed to give identifiable products. Next chemical oxidation of the monomer **1** was tried. Following the experimental procedure of Song [81], one equivalent of CF_3COOAg (1.06 V *vs*. AgCl/Ag) was mixed with **1** in CH_2Cl_2 for 10 min in the dark. The product was brown in color and the UV-vis spectra was not consistent with other known $[Fe^{III}Pc]^+$ species [22]. We think the pc ring was oxidized. We attempted to get EPR data at room temperature but only Ag^+ was visible in the EPR spectrum.

EXPERIMENTAL

General

The following materials were commercially available, and were used without purification: bromine, catechol, copper(I) cyanide, potassium carbonate, magnesium sulfate, DMF, toluene, THF, pyridine-d_5, 1,2,4,5-tetracyanobenzene and ferrous dichloride tetrahydrate. Pyridine was dried over calcium hydride, then vacuum transferred and stored in a dry box under prepurified nitrogen. *N*,*N* dimethylaminoethanol and 2-chloronaphthalene were freshly distilled whenever needed. Toluene, benzene and benzene-d_6 were dried over sodium, vacuum transferred and stored in a dry box under prepurified nitrogen. Ethanol, methanol, acetone, dichloromethane, and chloroform were dried by storage over activated 3 Å molecular sieves. KBr for IR spectra was kept in a desiccator when not in use.

Spectroscopy

^{1}H NMR spectra were taken on Varian UnityPlus 300 or AVANCE Bruker DPX400 or Varian INOVA500 instruments and were referenced to the appropriate solvent residual peaks. UV-vis spectra were taken on a Perkin-Elmer Lamba 11 UV-vis spectrometer. IR spectra were taken as KBr pellets or as thin films from evaporation of chloroform or ethanol on KBr salt plates and were measured on a Perkin-Elmer Paragon 1000 FTIR spectrometer.

Mass spectra were taken on a JEOL JUSAX505 HA mass spectrometer (ESI, FAB) or on a Voyager Perspective Biosystem mass spectrometer (MALDI). For ESI, the sample was dissolved in an electrospray solvent such as 50:50 v:v methanol:water with 2% acetic acid. This solution was passed through a metal capillary which was biased at high potential (4–5 kV). For MALDI, a 2,5-dihydroxybenzoic acid (DHBA) or α-cyano-4-hydroxycinnamic acid (ALPHA) MALDI matrix was dissolved in water or ethanol at a concentration of 20 mg/mL. The chloroform solution of **1** or **2** was mixed with the matrix in a ratio of 1:100 v/v in a 0.5 mL Eppendorf™ microtube. 1 μL of this mixture was deposited on the gold sample plate, dried at room temperature and then ionized by laser and analyzed. A nitrogen 32 UV Laser operating at 337 nm was used as the ionization source. Since chloroform and water are not miscible, the phthalocyanine signal was not evenly spread on the sample plate and we needed to move the ionization location around to maximize the signal.

HPLC

HPLC purification was done using a Waters™ alliance 2695 separation module along with a Waters™ 996 photodiode array detector. A Phenomenex™ LUNA silica column (250 × 4.6 mm, 100 Å) was used as the analytical HPLC column. A Phenomenex™ LUNA silica semi-prep column (250 × 10 mm, 100 Å) was used for large scale separation. 0.5 or 1 mL/min flow rates were used for analytical and semi-prep silica columns, respectively.

The eluent was an isocratic mixture of 2% pyridine in chloroform. Care should be taken to vent the eluent and its wastes to a fume hood.

Electrochemistry

Cyclovoltametric measurements were performed in a nitrogen-filled dry box using an EG&G instruments PAR 283 potentiostat/Galvanostat or BAS Epsilon EC instrument. A conventional three-electrode system was used. The working electrode was a 0.02 cm^2 Pt disk. An Ag/AgCl wire (soaked in 0.1 M tetrabutylammonium chloride(TBACl)/dichloromethane solution, 0.29 V *vs*. NHE or 0.044 V *vs*. SCE) was used as the reference electrode. All redox potentials were converted to the values *vs.* SCE. A platinum mesh spot welded to a platinum wire was used as the counter electrode. HPLC purified 1 (> 99%) and 2 (> 98%) were used for electrochemistry, typically at concentrations of 1 mM. Tetrabutylammonium tetrafluoroborate ($TBABF_4$, 0.1 M in CH_2Cl_2) served as the electrolyte. When pyridine was added, it was present in large excess (10 mM–1 M). Scan rates from 50 mV/s to 200 mV/s were used for cyclovoltammetry. In square wave voltammetry, the square wave amplitude and frequency were set to 50 mV and 50 Hz, respectively. The current full scale was 1 μA and a 1.0 Hz filter was used. The quiet time was set to 5 s and 1 millisecond was used as the sample period. For controlled-potential electrolysis of **2**, the potential was set to 1.5 V in order to get complete oxidation.

The cleanliness of the working electrode is very important to get good SW voltammograms. We used Pt disk electrodes consisting of a highly polished Pt wire embedded in a solvent-resistant chlorotrifluoroethylene (CTFE) plastic body. The small diameter of the wire (1.6 mm) gave a higher intensity of current than bare Pt or Au wires. It was important to polish the contacting end (diamond paste) before each experiment.

UV-vis titrations with pyridine

Samples of pure **1** and **2** were dried under vacuum on a Schlenk line for 2 h at room temperature at 20 mTorr to remove the pyridine residue from HPLC purification. Then, **1** (0.16 mg) or **2** (0.13 mg) was dissolved in 2.00 mL $CHCl_3$ in a UV-vis cuvette. The concentrations of **1** and **2** were 6.4×10^{-5} M and 3.1×10^{-5} M, respectively. Pyridine was added with a 10 μL glass syringe. Four kinds of pyridine solutions were made for injection: 0.1% (v/v) py/$CHCl_3$, 1% (v/v) py/$CHCl_3$, 10% (v/v) py/$CHCl_3$ and neat pyridine. At the end of each titration, a total of 130 μL solution had been added to the cuvette. Since the volume change was only 6%, we considered the concentration of the pc to be constant during the process.

Synthesis

1,2-Dibromocatechol (4). The synthesis procedure of this step followed Kohn's work [37]. Catechol (**3**) (55 g, 0.5 mol) was dissolved in 200 mL acetic acid and kept in an ice bath, and bromine (50 mL, 0.97 mol) was added *via* a dropping funnel over an hour. After the bromine was added, the reaction mixture was stirred for another 2 h on ice. After the solvent was removed by rotary evaporation, (CAUTION: HBr and HOAc are caustic; vacuum should be provided by an arrangement such as a diaphragm pump inside the ventilation hood to prevent HBr release to the lab) the brown oil was poured into 1.5 L ice-water. The precipitate was filtered, dried in air and recrystallized from toluene to give pale white crystals (52 g, 45% yield). ^{1}H NMR ($CDCl_3$): δ, ppm 7.16 (2H, s, Ar-H), 5.72 (2H, s, OH).

1,2-Dibromo-4,5-bis(pentyloxy)benzene (5). The synthesis procedure of this step followed Hanack *et al.* [36]. Dibromocatechol (**4**) (26.8 g, 0.10 mol) and potassium carbonate (20 g, 0.14 mol) were dissolved in 50 mL DMF, stirred for 30 min, then 1-bromopentane (25 mL, 0.21 mol), dissolved in 20 mL DMF, was added dropwise. The resulting brown solution was heated to 110 °C for 12 h, then the dark brown reaction solution was poured into 500 mL 0.2 N HCl and the product was extracted with 40 mL ether three times. The ether was removed by rotary evaporation, yielding 15 mL of brown oil. After recrystallization from ethanol, 34.2 g white crystals were obtained (85% yield). ^{1}H NMR ($CDCl_3$): δ, ppm 7.07 (2H, s), 3.95 (4H, t, J = 6.6 Hz), 1.82 (4H, m), 1.40 (8H, m), 0.92 (6H, t, J = 6.9 Hz). IR (thin film from ethanol): ν, cm^{-1} 2957 (vs), 2872 (vs), 1583 (m), 1498 (vs), 1468 (vs), 1387 (m), 1352 (s), 1329 (m), 1251 (vs), 1201 (vs), 1116 (m), 989 (m), 880 (m), 652 (m).

1,2-Dicyano-4,5-bis(pentyloxy)benzene (6). This synthesis followed van Nostrum's procedure [82]. CuCN (1.8 g, 150 mmol) was added to a solution of **5** (20.4 g, 50 mmol) in 120 mL DMF, and the solution was heated to 150 °C for 12 h under Ar. The green mixture was poured into 600 mL concentrated aqueous NH_4OH after it cooled down to RT, and air was bubbled through for 6 h. The green precipitate was filtered off and washed with water until the filtrate was neutral. After the solid air dried, it was extracted into 200 mL methanol in a Soxhlet extractor for 24 h. The product was crystallized from methanol (50 mL). It was purified by recrystallization in ethanol (30 mL) (white flaky crystals, 8.9 g, yield 59%). ^{1}H NMR ($CDCl_3$): δ, ppm 7.12 (2H, s), 4.05 (4H, t, J = 6.6 Hz), 1.86 (4H, m), 1.44 (8H, m), 0.94 (6H, t, J = 7.0 Hz). IR (thin film from CH_2Cl_2): ν, cm^{-1} 2228 (s, CN), 1590 (vs), 1526 (s), 1466 (m), 1394 (m), 1365 (m), 1293 (m), 1232 (vs), 1218 (s), 1095 (vs), 975 (m), 888 (m). MS (FAB): *m/z* calcd. 301 (100%) $[M + H]^+$, 302 (20%) found 301 (100%) $[M + H]^+$, 302 (25%), 275 $[M + HCN]^+$, 249 $[M + H_2CN]^+$, 162 $[M + H_2CN–OC_5H_{11}]^+$.

Bisdiiminoisoindoline (8). This process was modified from Piechocki's thesis [83]. The bis(diiminoisoindole) (**8**) was prepared by bubbling gaseous ammonia through 1,2,4,5-tetracyanobenzene (1.0 g) (**7**) in ethanol solution for 5 h. Since **8** has very low solubility in methanol,

it precipitated as a yellow powder (1.2 g, 100%) and was isolated by filtration. The reaction is conveniently followed by IR, as the peak at 2245 cm^{-1} (C≡N) of the starting material disappears. EI: *m/z* calcd. 212 (100%) $[M + H]^+$, 213 (13%), found 212 (100%) $[M + H]^+$, 213 (30%), 198 $[M + HN]^+$. IR (KBr pellet): ν, cm^{-1} 3359 (vs), 2950 (vs), 1686 (vs), 1560 (m), 1402 (vs), 1070 (m), 960 (s), 833 (s), 544 (s).

Side-by-side iron phthalocyanine dimer (2) and iron phthalocyanine monomer (1). The synthesis of these compounds followed the statistical method of Bossard's work on ruthenium phthalocyanines [84]. A 50 mL three neck flask was filled with bisdiiminoisoindoline (0.038 g, 0.18 mmol) (**8**) and 10 mL of DMAE and heated to boiling temperature under nitrogen. The reaction was set to reflux through one neck under a slow nitrogen purge (to a gas bubbler). The other two necks were sealed with SUBASEAL™ rubber stoppers. Ferrous dichloride tetrahydrate ($FeCl_2 \cdot 4H_2O$, 0.066 g, 0.33 mmol) was boiled in 5 mL of DMAE for 5 min until all the water had distilled out. The iron solution was added slowly over 20 min through one neck of the flask using a syringe and the syringe was rinsed with a little DMAE to ensure quantitative transfer. Simultaneously, through the other neck, excess (0.30 g, 1.00 mmol) 1,2-dicyano-4,5-bis(pentyloxy)benzene (**6**) in 5 mL of DMAE was added in 20 min using another syringe. After all the ingredients were added, the syringes were removed, the nitrogen was turned off, and a long needle was connected to an ammonia gas tank *via* a gas trap (to prevent any suckback of the reaction mixture into the tank) to introduce ammonia into the reaction flask. The resulting brown suspension was gently refluxed under a slow bubbling of ammonia gas for 3 days. After cooling to room temperature, 100 mL of ethanol was added to precipitate the phthalocyanine products. After washing in a Soxhlet extractor with acetone and methanol for 2 days each, the phthalocyanine products were extracted into 100 mL chloroform until the Soxhlet extracts were water white. After evaporation of the chloroform, a green solid (299 mg) was obtained. This green solid was first purified by gel-permeation chromatography (BioBeads SX1) using toluene as eluent.

The first fraction was collected from the GPC column and the toluene was removed by rotary evaporation (80 mg crude). It contained about 50% **2** and 50% **1**. HPLC was used to do further purification using 2% pyridine in chloroform as the eluent. A Phenomenex™ LUNA normal phase silica analytical column (250 × 4.6 mm, 100 Å) was used to identify and quantify compounds **1** and **2**. The flow rate was set to 0.5 mL/second. Two major components were observed at retention times of 5.7 and 6.7 min, and by UV-vis measurements and mass spectrometry, these fractions were identified as compounds **1** and **2**, respectively. Multiple injections were performed on the semi-prep HPLC column. The flow rate was set to 1 mL/second. Peaks eluted at 26.5 and 30 min, which corresponded to compounds **1** and **2**, respectively. **2** was checked by analytical HPLC to confirm its purity (> 98% measured at 699 nm). The yield of pure **2** (38 mg) was 12% based on tetracyanobenzene. Even after prolonged drying under 20 mTorr vacuum on a Schlenk line, pyridine from the HPLC separation seems to be present in both **1** and **2** (as seen in the NMR) and we cannot rule out the presence of other impurities that are NMR and HPLC silent. The UV spectrum was measured in neat pyridine solution to get characteristic isolated phthalocyanine absorption peaks. **2.** ^1H NMR ($CDCl_3$): δ, ppm 9.74 (2H, s), 8.72 (4H, s), 8.69 (4H, s), 8.68 (4H, s), 4.55-4.37 (24H, m), 2.12 (24H, m), 1.70 (24H, m), 1.53 (24H, m), 1.03 (36H, m). MS (MALDI): *m/z* calcd. 2093 (100%) $[M + H]^+$, found 2093 (100%) $[M + H]^+$ (pyridine coordination was often found in the MALDI spectrum due to the use of pyridine in the eluent). UV-vis (in pyridine): λ_{max}, nm 339 (Soret band, $\varepsilon = 4.98 \times 10^4$), 633, 699 (Q-band, $\varepsilon = 3.68 \times 10^4$).

The second green fraction coming out of the column was **1** (2,3,9,10,16,17,23,24-octakis(pentyloxy)iron-phthalocyanine, 90 mg, 29%). Its purity (99%) was measured by HPLC with 2% pyridine in chloroform as the eluent. Its UV spectrum was measured in neat pyridine solution to get characteristic isolated phthalocyanine absorption peaks. **1.** ^1H NMR ($CDCl_3$): δ, ppm 8.66 (8H, s), 4.42 (16H, t), 2.17 (16H, m), 1.50 (32H, m), 0.92 (24H, t). MS (MALDI): *m/z* calcd. 1257.99 $[M + H]^+$, found 1254.43 $[M + H]^+$, 1274 $[M + NH_3]^+$, 1291 $[M + 2NH_3]^+$, 1215 $[M + H–C_3H_7]^+$, 1185 $[M + H–C_5H_{11}]^+$, 1170 $[M + H–OC_5H_{11}]^+$. UV-vis (in pyridine): λ_{max}, nm 342 (Soret band, $\varepsilon = 1.66 \times 10^4$), 430, 598, 630, 660 (Q-band, $\varepsilon = 1.32 \times 10^4$).

CONCLUSION

A new side-by-side iron phthalocyanine dimer (**2**) was synthesized with peripheral substituents that render it soluble in organic solvents. After purification by gel permeation chromatography and HPLC, a 12% yield of the desired product in 98% pure form was obtained, along with a major side product, the monomeric iron phthalocyanine **1**. There are a few novel aspects of this new side-by-side pc dimer. First, this is a new compound with full pentyloxy substitution (-O-C_5H_{11}), which gives high solubility in organic solvents and a well behaved NMR. Second, it was purified mainly by HPLC, which is rarely used in pc purification but has great potential. The usage of the photodiode array detector with HPLC data greatly helped the purification process. Third, the synthesis used NH_3 as a protection gas to improve the yield of the side-by-side pc dimer. With the addition of pyridine, their NMR spectra of both monomer and dimer became much clearer, and their UV-vis spectra indicated a multiphase aggregation in DCM solution that was broken up as pyridine coordinated to the axial positions

of the iron pc. Oxidation of the Fe was associated with loss of coordinated pyridine. Considering that we may need to use an axial ligand like pyridine to help graft the cationic mixed-valence $\mathbf{2}^{+}$ (product of reaction I) to a surface, this result indicates that the anionic mixed-valence $\mathbf{2}^{-}$ (product of reaction II) may be a better candidate as a mixed-valence compound for the molecular QCA project. It remains to be seen whether the Fe-Pc-pyridine linkage in molecules of $\mathbf{2}^{+}$ might be stable for dry surface-bound molecules.

Acknowledgements

We thank Dr. David Alonso (Andrews University) and his students Marco Allard, James Fox and William Hardesty for useful discussions. The National Science Foundation supported this work financially (NSF CCF0403760).

Supporting information

Full separation and characterization information for **1** and **2** are given in the supplementary material. This material is available free of charge *via* the Internet at http://www.worldscinet.com/jpp/jpp.shtml.

REFERENCES

1. Lent CS, Isaksen B and Lieberman M. *J. Am. Chem. Soc.* 2003; **125**: 1056–1063.
2. Lent CS, Tougaw PD and Porod W. *Proc. Workshop on Physics and Computing*, IEEE Computer Society Press, 1994; 5–13.
3. Lieberman M, Chellamma S, Varughese B, Wang Y, Lent C, Bernstein G, Snider G and Peiris F. *Mol. Electron. II, Ann. New York Acad. Sci.* 2002; **960**: 225–239.
4. Ellenbogen JC and Love JC. *Proc. IEEE* 2000; **88**: 386–426.
5. Li M, Schnablegger H and Mann S. *Nature* 1999; **402**: 393–395.
6. Loweth CJ, Caldwell WB, Peng XG, Alivisatos AP and Schultz PG. *Angew. Chem., Int. Ed.* 1999; **38**: 1808–1812.
7. Norris DJ and Vlasov YA. *Adv. Mater.* 2001; **13**: 371–376.
8. Hu WC, Sarveswaran K, Lieberman M and Bernstein GH. *J. Vac. Sci. Technol., B* 2004; **22**: 1711–1716.
9. Lowery MK, Starshak AJ, Esposito JN, Krueger PC and Kenney ME. *Inorg. Chem.* 1965; **4**: 128.
10. Pawlowski G and Hanack M. *Synth. Stuttgart* 1980: 287–289.
11. Caminiti R, Donzello MP, Ercolani C and Sadun C. *Inorg. Chem.* 1999; **38**: 3027–3029.
12. Ceyhan T, Altindal A, Ozkaya AR, Erbil MK, Salih B and Bekaroglu Z. *Chem. Commun.* 2006: 320–322.
13. Kleinwachter J and Hanack M. *J. Am. Chem. Soc.* 1997; **119**: 10684–10695.
14. Asano Y and Kobayashi N. *Tetrahedron Lett.* 2004; **45**: 9577–9580.
15. Dominguez DD, Snow AW, Shirk JS and Pong RGS. *J. Porphyrins Phthalocyanines* 2001; **5**: 582–592.
16. Lelievre D, Bosio L, Simon J, Andre JJ and Bensebaa F. *J. Am. Chem. Soc.* 1992; **114**: 4475–4479.
17. Li ZY. *Ph.D. Thesis*, University of Notre Dame: South Bend, IN, 2001.
18. Li ZY and Lieberman M. *Inorg. Chem.* 2001; **40**: 932–939.
19. Wang YL. and Lieberman M. *IEEE Trans. Nanotechnol.* 2004; **3**: 368–376.
20. Janczak J and Kubiak R. *Inorg. Chim. Acta* 2003; **342**: 64–76.
21. Kennedy BJ, Murray KS, Zwack PR, Homborg H and Kalz W. *Inorg. Chem.* 1985; **24**: 3302–3305.
22. Kobayashi N, Koshiyama M, Funayama K, Osa T, Shirai H and Hanabusa K. *J. Chem. Soc.: Chem. Commun.* 1983: 913–914.
23. Kobayashi N, Kondo R, Nakajima S and Osa T. *J. Am. Chem. Soc.* 1990; **112**: 9640–9641.
24. Kobayashi N, Ishizaki T, Ishii K and Konami H. *J. Am. Chem. Soc.* 1999; **121**: 9096–9110.
25. Weitemeyer A, Kliesch H and Wohrle D. *J. Org. Chem.* 1995; **60**: 4900–4904.
26. Kobayashi N, Muranaka A and Nemykin VN. *Tetrahedron Lett.* 2001; **42**: 913–915.
27. Kobayashi N, Miwa H and Nemykin VN. *J. Am. Chem. Soc.* 2002; **124**: 8007–8020.
28. Kimura M, Kuroda T, Ohta K, Hanabusa K, Shirai H and Kobayashi N. *Langmuir* 2003; **19**: 4825–4830.
29. Maya EM, Vazquez P and Torres T. *Chem. Eur. J.* 1999; **5**: 2004–2013.
30. Nakagawa M, Rikukawa M, Sanui K and Ogata N. *Synth. Met.* 1997; **84**: 391–392.
31. Alonso C, Pascual MJ, Salomon AB, Abruna HD, Gutierrez A, Lopez MF, Garcia-Alonso MC and Escudero ML. *J. Electroanal. Chem.* 1997; **435**: 241–254.
32. Kobayashi N, Higashi Y and Osa T. *Chem. Lett.* 1994: 1813–1816.
33. Kobayashi N, Lam H, Nevin WA, Janda P, Leznoff CC, Koyama T, Monden A and Shirai H. *J. Am. Chem. Soc.* 1994; **116**: 879–890.
34. Yang J and Vandemark MR. *Tetrahedron Lett.* 1993; **34**: 5223–5226.
35. Ferencz A, Neher D, Schulze M, Wegner G, Viaene L and De Schryver FC. *Chem. Phys. Lett.* 1995; **245**: 23–29.
36. Hanack M, Gul A, Hirsch A, Mandal BK, Subramanian LR and Witke E. *Mol. Cryst. Liq. Cryst.* 1990; **187**: 365–382.
37. Kohn M. *J. Am. Chem. Soc.* 1951; **73**: 480–480.
38. Freas RB and Campana JE. *Inorg. Chem.* 1984; **23**: 4654–4658.

39. Bo SH, Tang DH, Liu XH and Zhen Z. *Dyes Pigm.* 2008; **76**: 35–40.
40. Fukuda T, Homma S and Kobayashi N. *Chem. Eur. J.* 2005; **11**: 5205–5216.
41. Giribabu L, Kumar CV, Reddy VG, Reddy PY, Rao CS, Jang SR, Yum JH, Nazeeruddin MK and Gratzel M. *Sol. Energy Mater. Sol. Cells* 2007; **91**: 1611–1617.
42. Vagin SI, Frickenschmidt A, Kammerer B and Hanack M. *Chem. Eur. J.* 2005; **11**: 6568–6573.
43. Bornsen KO and Mohr MD. *Anal. Methods Instrum.* 1995; **2**: 158–160.
44. Knochenmuss R, Stortelder A, Breuker K and Zenobi R. *J. Mass Spectrom.* 2000; **35**: 1237–1245.
45. Wilkinson WR, Gusev AI, Proctor A, Houalla M and Hercules DM. *Fresenius J. Anal. Chem.* 1997; **357**: 241–248.
46. Chen MJ, Nunez L, Rathke JW and Rogers RD. *Organomet.* 1996; **15**: 2338–2344.
47. Tse YH, Seymour P, Kobayashi N, Lam H, Leznoff CC and Lever ABP. *Inorg. Chem.* 1991; **30**: 4453–4459.
48. Edwards L and Gouterma M. *J. Mol. Spectrosc.* 1970; **33**: 292.
49. Henrikss A and Sundbom M. *Theor. Chim. Acta* 1972; **27**: 213.
50. Jerwin K and Wasgestian F. *Spectrochim. Acta, Part A.: Mol. and Biomol. Spectrosc.* 1984; **40**: 159–163.
51. Dodsworth ES, Lever ABP, Seymour P and Leznoff CC. *J. Phys. Chem.* 1985; **89**: 5698–5705.
52. Kane AR, Sullivan JF, Kenny DH and Kenney ME. *Inorg. Chem.* 1970; **9**: 1445.
53. Snow AW and Jarvis NL. *J. Am. Chem. Soc.* 1984; **106**: 4706–4711.
54. Kobayashi N and Lever ABP. *J. Am. Chem. Soc.* 1987; **109**: 7433–7441.
55. Nozawa T, Kobayashi N, Hatano M, Ueda M and Sogami M. *Biochim. Biophys. Acta* 1980; **626**: 282–290.
56. Nyokong T, Gasyna Z and Stillman MJ. *Inorg. Chem.* 1987; **26**: 1087–1095.
57. Vancott TC, Rose JL, Misener GC, Williamson BE, Schrimpf AE, Boyle ME and Schatz PN. *J. Phys. Chem.* 1989; **93**: 2999–3011.
58. Janczak J and Kubiak R. *Crystengcomm* 2010; **12**: 3599–3606.
59. Stillman MJ and Thomson AJ. *J. Chem. Soc.: Faraday Trans. II* 1974; **70**: 790–804.
60. Kobayashi H and Yanagawa Y. *Bull. Chem. Soc. Jpn* 1972; **45**: 450.
61. Hush NS and Woolsey IS. *Mol. Phys.* 1971; **21**: 465.
62. Kobayashi N, Fukuda T and Lelievre D. *Inorg. Chem.* 2000; **39**: 3632–3637.
63. Leznoff CC, Lam H, Nevin WA, Kobayashi N, Janda P and Lever ABP. *Angew. Chem., Int. Ed.* 1987; **26**: 1021–1023.
64. Makarov S, Litwinski C, Ermilov EA, Suvorova O, Roder B and Wohrle D. *Chem. Eur. J.* 2006; **12**: 1468–1474.
65. De La Torre G, Martinez-Diaz MV and Torres T. *J. Porphyrins Phthalocyanines* 1999; **3**: 560–568.
66. Kobayashi N and Ogata H. *Eur. J. Inorg. Chem.* 2004: 906–914.
67. Kennedy BJ, Murray KS, Zwack PR, Homborg H and Kalz W. *Inorg. Chem.* 1986; **25**: 2539–2545.
68. Kuppers H, Eulert HH, Hesse KF, Kalz W and Homborg H. *Z. Naturforsch., B: J. Chem. Sci.* 1986; **41**: 44–47.
69. Kuppers H, Kalz W and Homborg H. *Acta Crystallogr., Sect. C: Cryst. Struct. Commun.* 1985; **41**: 1420–1423.
70. Lam H, Marcuccio SM, Svirskaya PI, Greenberg S, Lever ABP, Leznoff CC and Cerny RL. *Can. J. Chem.: Rev. Can. Chim.*1989; **67**: 1087–1097.
71. Piechocki C and Simon J. *J. Chem. Soc.: Chem. Commun.* 1985: 259–260.
72. Gok Y and Yildiz SZ. *Polyhedron* 1997; **16**: 2335–2339.
73. Yeung YO, Liu RCW, Law WF, Lau PL, Jiang JZ and Ng DKP. *Tetrahedron* 1997; **53**: 9087–9096.
74. Gottlieb HE, Kotlyar V and Nudelman A. *J. Org. Chem.* 1997; **62**: 7512–7515.
75. Ishii K, Kobayashi N, Higashi K, Osa T, Lelievre D, Simon J and Yamauchi S. *Chem. Commun.* 1999: 969–970.
76. Lever ABP. *J. Porphyrins Phthalocyanines* 1999; **3**: 488–499.
77. Lever ABP, Milaeva ER and Speier G. *Phthalocyanines, Properties and Applications*, Vol. 3, VCH: NY, 1983; pp 1–70.
78. Wolberg A and Manassen J. *J. Am. Chem. Soc.* 1970; **92**: 2982–2991.
79. Campbell RH, Heath GA, Hefter GT and McQueen RCS. *J. Chem. Soc.: Chem. Commun.* 1983: 1123–1125.
80. Lever ABP and Wilshire JP. *Inorg. Chem.* 1978; **17**: 1145–1151.
81. Song L and Trogler WC. *Angew. Chem. Int. Ed.* 1992; **31**: 770–772.
82. van Nostrum CF, Picken SJ, Schouten AJ and Nolte RJM. *J. Am. Chem. Soc.* 1995; **117**: 9957–9965.
83. Piechocki C. *Ph.D. Thesis*, University of Paris, Paris, 1985.
84. Bossard GE, Abrams MJ, Darkes MC, Vollano JF and Brooks RC. *Inorg. Chem.* 1995; **34**: 1524–1527.